Supplementary Information (SI) for Chemical Science.

Electronic Supplementary Information (ESI)

Synergistic intercalation-conversion reaction mechanism in Prussian blue analogue materials toward enhanced Na storage

Na Liu$^+$, Xiaohan Wang$^+$, Jing Liu, Ningbo Liu, and Liubin Wang*

College of Chemistry and Materials Science, Key Laboratory of Analytical Science and Technology of Hebei Province, Hebei Research Center of the Basic Discipline of Synthetic Chemistry, Hebei University, Baoding, Hebei 071002, China

$^+$The authors contribute equally to this work.

Corresponding Author

*Liubin Wang (E-mail: lbwang@hbu.edu.cn)

Contents

19. Fig. S18: XRD patterns of PbHCF/CNTs electrode at different cycles.

20. Fig. S19: XPS Pb 4f and Fe 2p spectra of PbHCF/CNTs in different charging and discharging states.

21. Fig. S20: Cycling performance of HC||PbHCF/CNTs full cell at 50 mA g^{-1}.

22. Table S1: Atomic coordinates of PbHCF.

23. Table S2: ICP-OES results of PbHCF/CNTs.

24. Table S3: Comparison of PbHCF/CNTs sample with reported PBA-based cathodes in SIBs.

Experimental section

Material synthesis

All chemical reagents used in this study were of analytical grade and employed without further purification. Prior to synthesis, multi-walled carbon nanotubes (CNTs, 40-60 nm diameter) were purified via refluxing in 6 M HNO_3 at 140 °C for 48 h to remove impurities and improve aqueous dispersibility. with fluxed at 120 °C in the mixed acid of concentrated sulfuric and nitric acid solutions with a ratio of 3:1 for 12 h to eliminate impurities and enhance their dispersibility in water. For the typical synthesis of PbHCF/CNTs, 25 mg of pretreated CNTs were ultrasonically dispersed in 20 mL deionized water for 30min to form a homogeneous suspension. Subsequently, 0.8 mmol $Pb(NO_3)_2$ (0.2650 g) was added to the CNTs suspension under continued ultrasonication for 30 min, yielding Solution A. Meanwhile, 0.4 mmol $K_4Fe(CN)_6 \cdot 3H_2O$ (0.4492 g) and 21.46 mmol KCl (1.600 g) were dissolved in 20 mL deionized water under vigorous stirring for 10 min, forming solution B. Solution B was then added dropwise to solution A with continuous stirring at 70 ℃ for 1 h. The resulting PbHCF/CNTs composite was aged at room temperature for 24 h, after which the black product was collected by centrifugation, washed with deionized water and ethanol for several times, and dried in a vacuum oven at 60 °C for 12 hours. PbHCF was synthesized using the same procedure, excluding the introduction of CNTs.

Material characterizations

Crystallographic analysis was performed using a Bruker D8 Advance X-ray diffractometer (Cu Kα radiation, $\lambda = 1.5406$ Å) with 2θ ranging from 10° to 70° at 6° min^{-1}. Morphological characterization was conducted via field-emission scanning electron microscopy (SEM, JEOL JSM-7800F) and transmission electron microscopy (TEM, FEI TECNAI G2) with elemental mapping capabilities. Raman spectra were acquired on a Thermo Scientific DXR spectrometer (532 nm laser excitation). Chemical bonding analysis utilized a Bruker ALPHA Fourier-transform infrared (FTIR) spectrometer equipped with an ATR accessory. Surface chemistry was probed by X-ray photoelectron spectroscopy (XPS, Perkin Elmer PHI 1600 ESCA) with monochromatic Al Kα radiation (1486.6 eV). Thermogravimetric analysis (TGA) was performed on a NETZSCH STA449C instrument under air flow (35-800 °C, 10 °C min^{-1}), revealing 11 wt% carbon content in the composite.

Electrochemical measurement

Electrodes were prepared by homogenously blending active material (PbHCF/CNTs or PbHCF), conductive carbon, and poly(vinylidene fluoride) (PVDF) binder (8:1:1 mass ratio) in N-methyl-2-pyrrolidone solvent. The resultant slurry was cast onto aluminum foil current collectors and vacuum-dried at 80 °C for 12 h, followed by punching into 12 mm diameter discs. CR20232 coin cells were assembled in an Ar-filled glovebox (Mikrouna, $O_2/H_2O \leq 0.01$ ppm) using the prepared working electrode, a pure Na foil (12 mm diameter) as the counter electrode, a porous glass fiber separator and 1 M $NaClO_4$ in propylene carbonate (PC) with 5% Fluoroethylene carbonate (FEC) additive as the electrolyte. In the assembly of the HC||PbHCF/CNTs full-cell, both HC and PbHCF/CNTs electrodes underwent three activation cycles to establish a stable surface/interface. The full battery, maintaining a N/P capacity ratio of 1: 1.2, operates within a voltage range of 0.9 to 3.8 V. Galvanostatic charge/discharge tests (GCD) were carried out in the voltage range of 1.1-3.8 V vs. Na^+/Na using a LAND battery tester (CT2001A). Cyclic voltammetry measurements (CV) were performed on electrochemical workstation (CHI760E) at a scan rate of 0.1 mV s^{-1}. Electrochemical impedance spectroscopy (EIS) spectrum of the PbHCF/CNTs and PbHCF electrodes was recorded over a frequency range from 0.01 Hz to 100 kHz. For the galvanostatic intermittent titration technique (GITT) measurements, the cells were discharged at 20 mA g^{-1} for 30 min, followed by a relaxation process under open circuit conditions for 2 h.

Calculation

Density functional theory (DFT) calculations were performed using the Vienna abinitio simulation package (VASP) with spin-polarized generalized gradient approximations (GGA) based on the Perdew, Burke, and Ernzerhof (PBE) scheme to model exchange and correlation effects.[1,2] A kinetic cutoff energy of 450 eV was applied for both geometry optimization and self-consistent field computation. The k-point was set to be 3 × 2 × 2. Structural optimizations proceeded until energy convergence reached 10^{-5} eV with residual forces below 0.02 eV Å^{-1}.

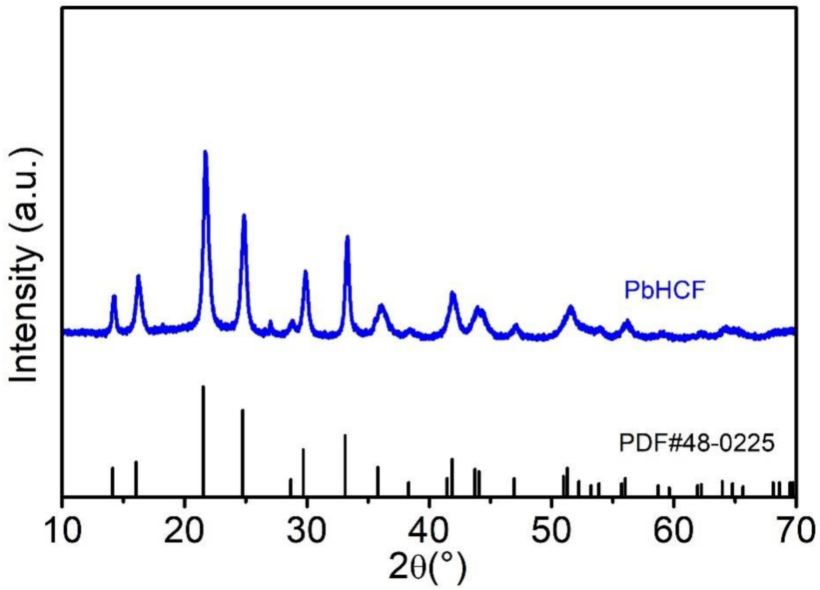

Fig. S1. XRD patterns of pristine PbHCF.

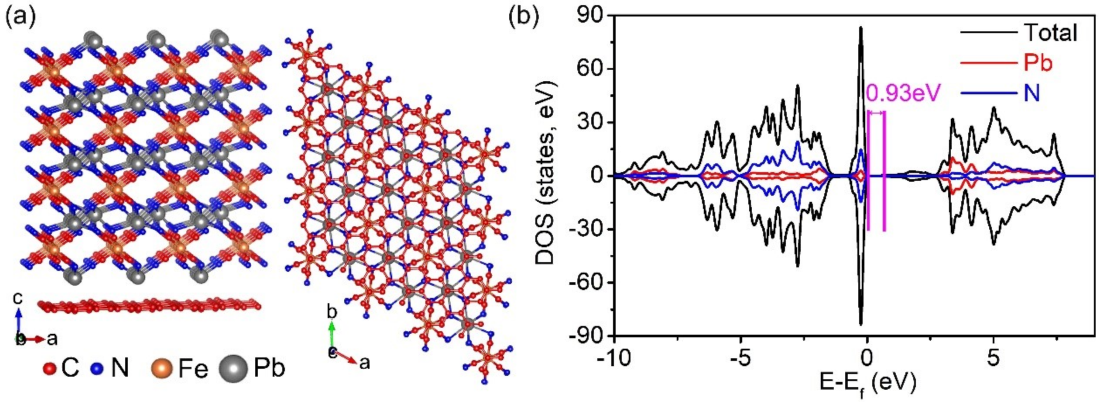

Fig. S2. Crystal structure and DOS of PbHCF/CNTs.

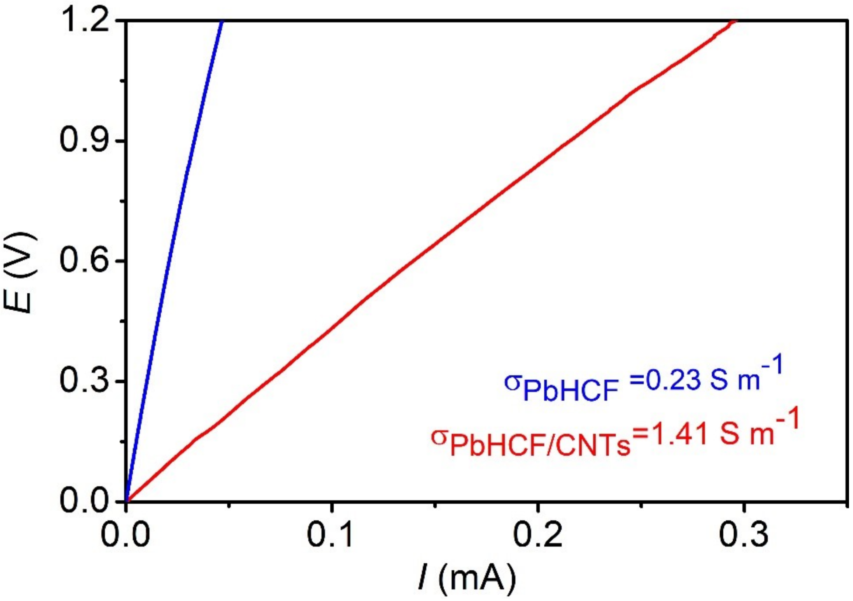

Fig. S3. I-V curves for PbHCF and PbHCF/CNTs.

Calculation of electrical conductivity: The electric conductivity was measured by using two-terminal devices, in which the material itself was pressed into pellets. The samples showed similar I-V curves suggesting quasi-Ohmic contacts. The resistances of PbHCF/CNTs and PbHCF samples are 4.01 Ω and 24.59 Ω, respectively. The area of the pellets is about 0.518 cm^2, and the electric conductivity of PbHCF/CNTs and PbHCF are calculated to be 1.41 S m^{-1} and 0.23 S m^{-1}, respectively.

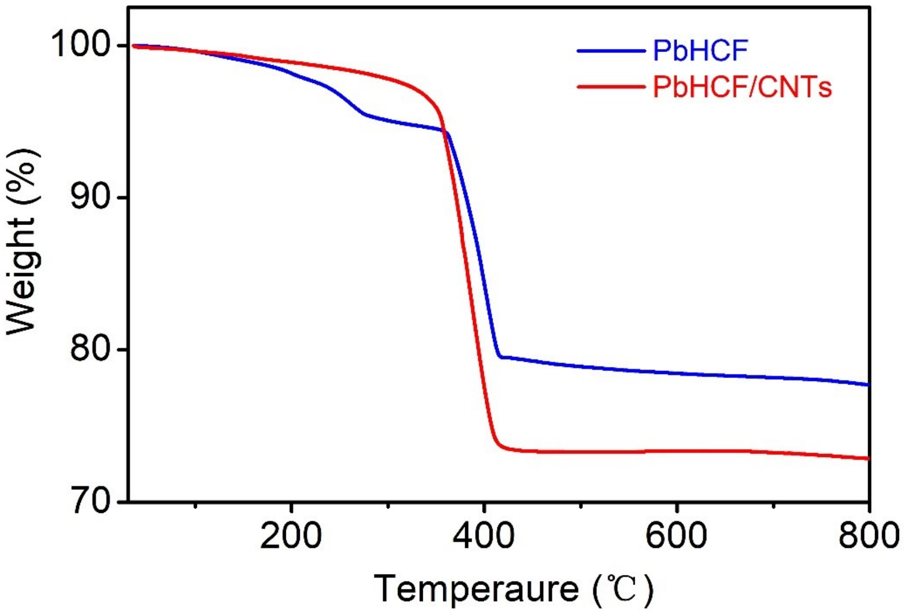

Fig. S4. Thermogravimetric curves of PbHCF and PbHCF/CNTs.

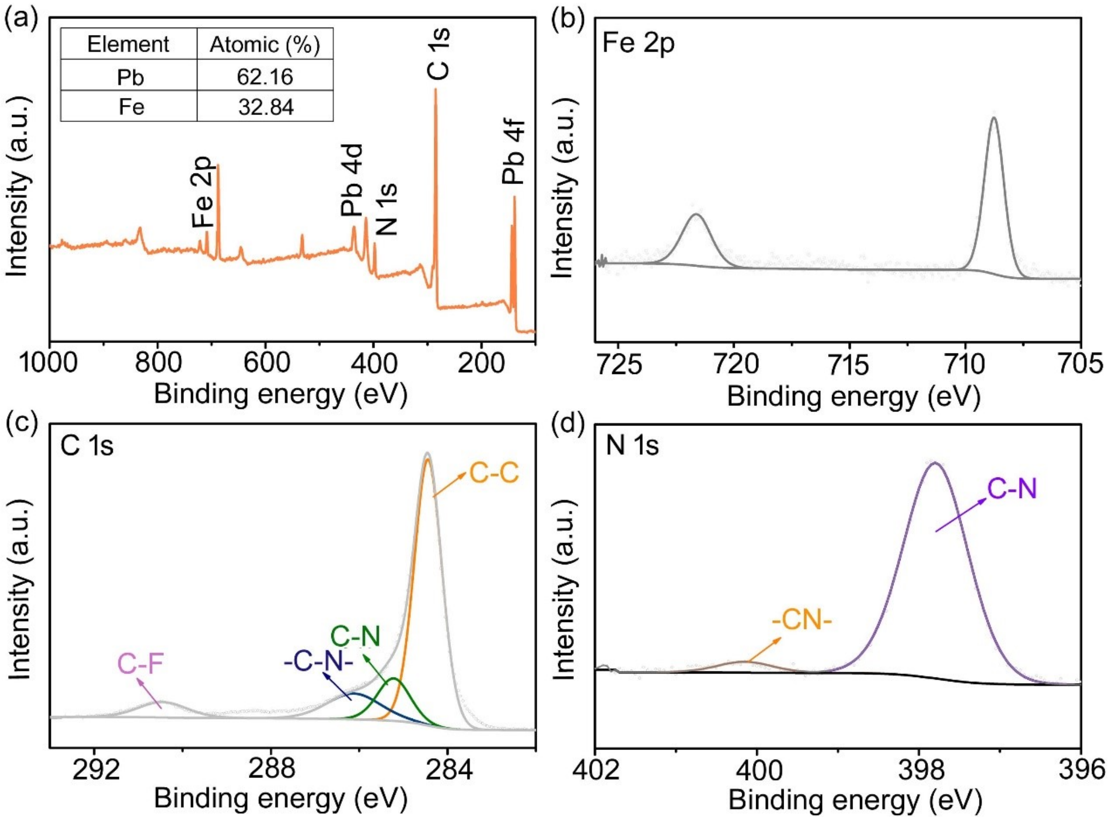

Element	Atomic (%)
Pb	62.16
Fe	32.84

Fig. S5. XPS survey, Fe 2p, N 1s and C 1s spectra of PbHCF/CNTs.

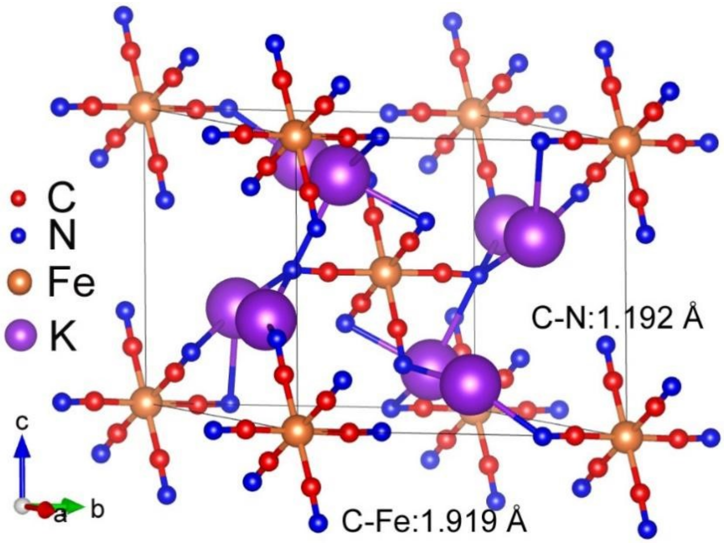

Fig. S6. Diagram of the coordination structure and bond length of $K_4Fe(CN)_6$.

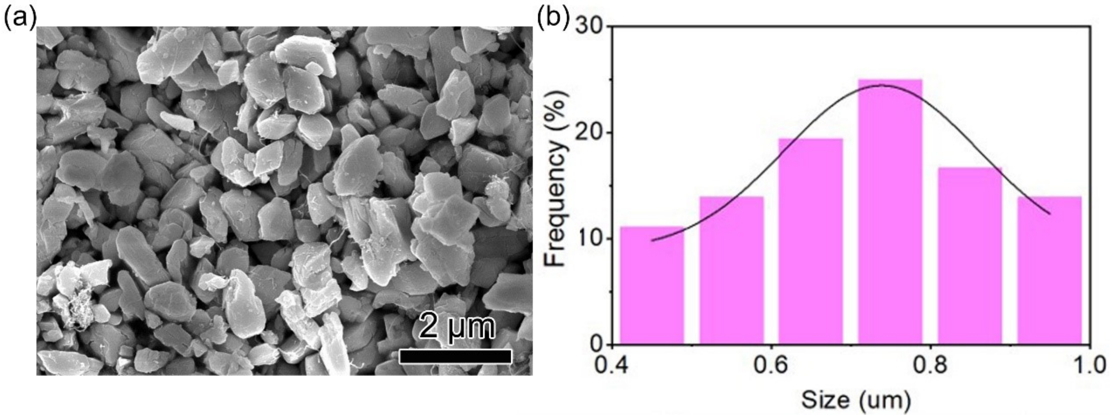

Fig. S7. SEM images of PbHCF/CNTs and the corresponding particle size distribution.

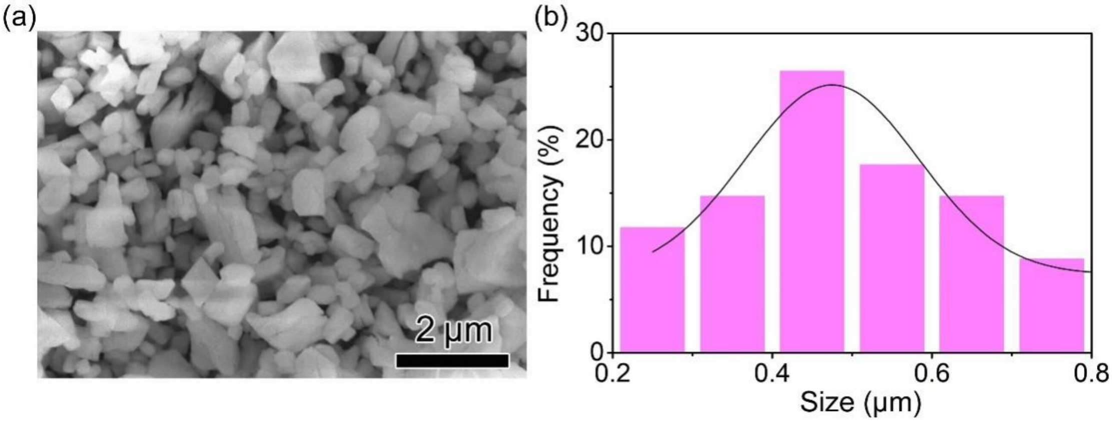

Fig. S8. SEM images of PbHCF and the corresponding particle size distribution.

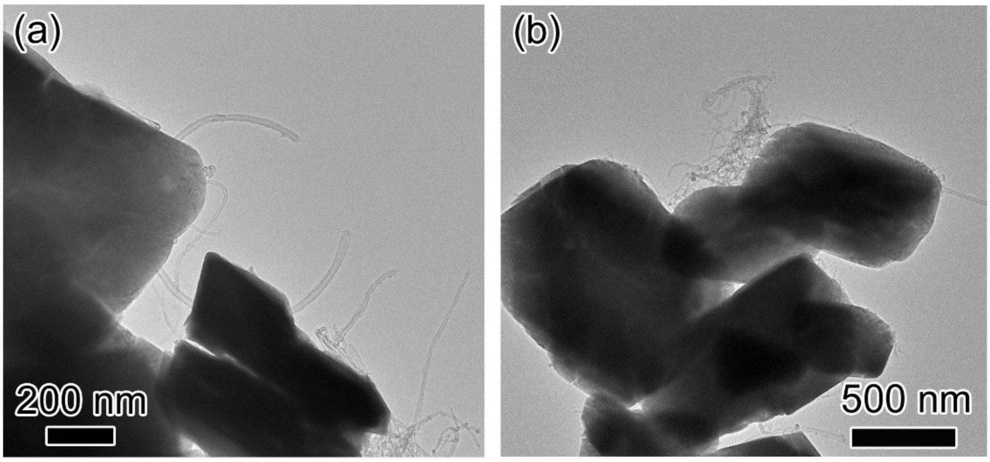

Fig. S9. TEM images of PbHCF/CNTs.

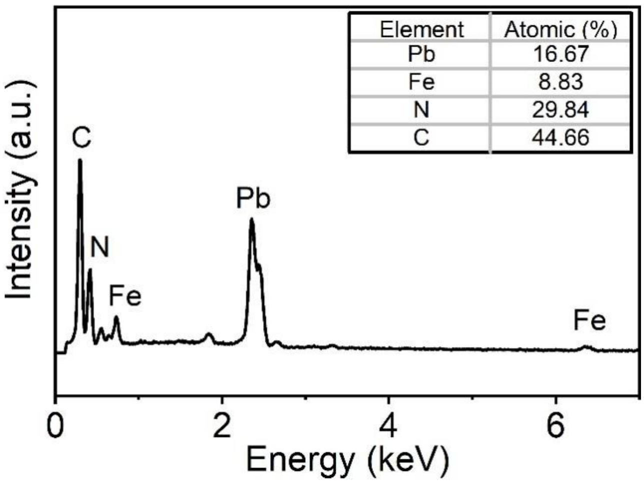

Element	Atomic (%)
Pb	16.67
Fe	8.83
N	29.84
C	44.66

Fig. S10. Energy dispersive X-ray spectroscopy of PbHCF/CNTs and the corresponding atomic fraction.

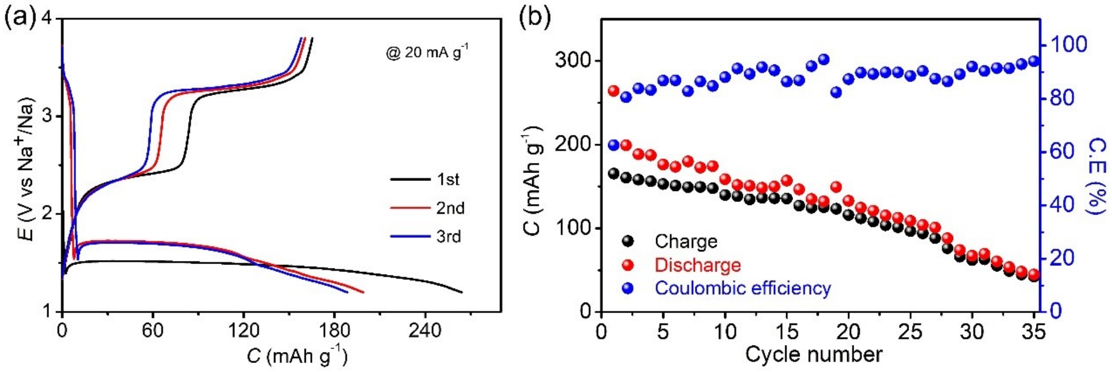

Fig. S11. Charge/discharge curves of PbHCF at 20 mA g^{-1}.

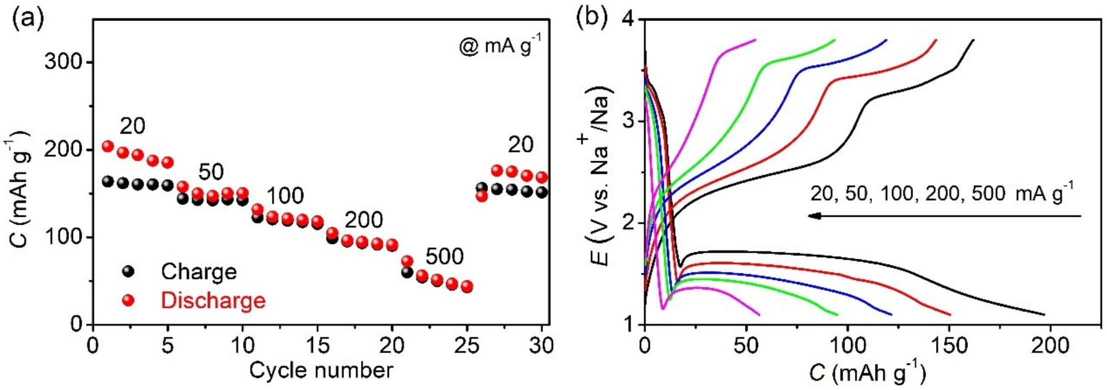

Fig. S12. Rate capacity of PbHCF/CNTs at current rates ranging from 20 mA g^{-1} to 500 mA g^{-1}.

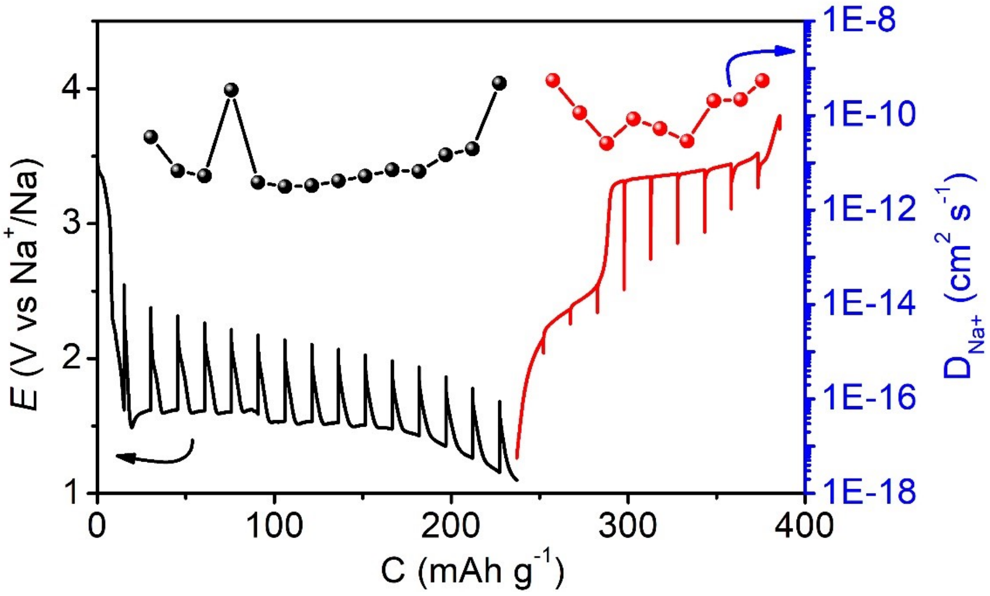

Fig. S13. GITT curves and the corresponding calculated diffusion coefficients during discharge/charge process of PbHCF/CNTs electrode.

Calculation of diffusion kinetics: In our study, the current pulse lasted for 30 min at 20 mA g^{-1} and then the cell was relaxed for 120 min to make the voltage reach the equilibrium. These procedures were repeatedly applied to the cell during the entire discharge/charge process. The Na$^+$ diffusion coefficients in the PbHCF/CNTs cathode were calculated from the GITT data by following formula:

$$D_{GITT} = \frac{4}{\pi}\left(\frac{m_B V_m}{M_B S}\right)^2\left(\frac{\Delta E_s}{\tau(dE_\tau/d\sqrt{\tau})}\right)^2 \approx \frac{4}{\pi\tau}\left(\frac{m_B V_m}{M_B S}\right)^2\left(\frac{\Delta E_s}{\Delta E_\tau}\right)^2\left(\tau \ll \frac{L^2}{D_{GITT}}\right)$$

Where D_{Na+} (cm^2 s^{-1}) means the chemical diffusion coefficient, τ is the constant current duration time (20 min), M_B is the mass of active material, M_B is the molecular weight (g mol^{-1}) and V_m is its molar volume (cm^3 mol^{-1}), S is the total contacting area of electrode with electrolyte (1.13 cm^2), and ΔE_s and ΔE_τ are the change in the steady state voltage and overall cell voltage after the application of a current pulse in a single step GITT experiment, respectively.

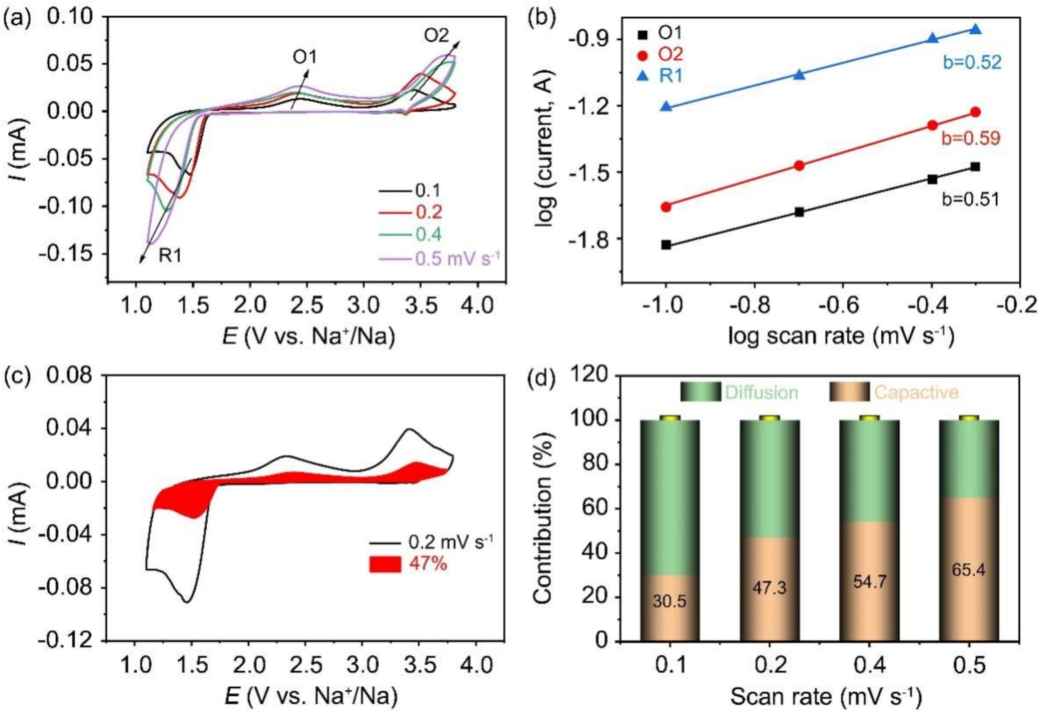

Fig. S14. (a) CV curves of PbHCF/CNTs at scan rates from 0.1-0.5 mV s^{-1}; (b) relationship between different peak currents and scan rates of PbHCF/CNTs; (c) The separation between total charge storage and capacitance control contribution at 0.1 mV s^{-1}; (d) the capacitive contributions at varying scan speeds.

The relationship between peak current (i_p) and scanning rate (v) can be described by the following formula: $i_p = a^v b$ ($\lg i_p = \lg a + b \lg v$), where a and b are adjustable parameters. The linear relationship between the peak current and the scanning rate is shown in Fig. S14b. The b values of O1, O2 and R1 are 0.51 0.59 and 0.52 respectively, indicating that the charge storage process is controlled by faraday intercalation. When the scanning rate is 0.2 mV s^{-1}, the red shaded area accounts for 47.3% of the total charge storage (Fig. S14c). Obviously, as the scanning rate increases, the capacitive effect gradually takes the lead (Fig. S14d), indicating that PbHCF/CNTs can promote rapid charge transfer and enhance the diffusion ability of Na^+.

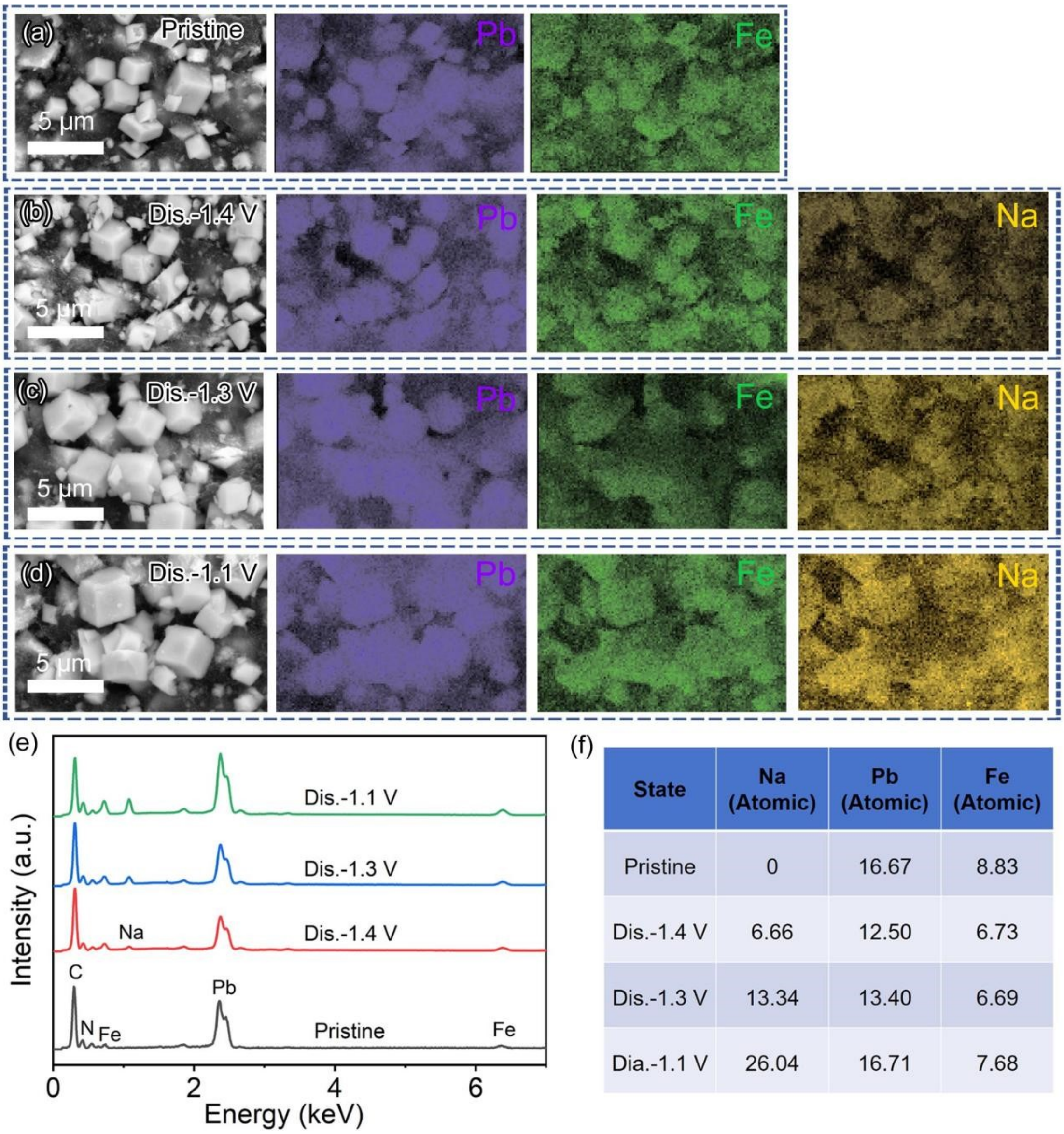

State	Na (Atomic)	Pb (Atomic)	Fe (Atomic)
Pristine	0	16.67	8.83
Dis.-1.4 V	6.66	12.50	6.73
Dis.-1.3 V	13.34	13.40	6.69
Dia.-1.1 V	26.04	16.71	7.68

Fig. S15. SEM elemental mapping images of the PbHCF/CNTs electrodes at (a) pristine, (b-d) different discharge states; the corresponding (e) energy dispersive X-ray spectroscopy analysis and (f) element content ratios.

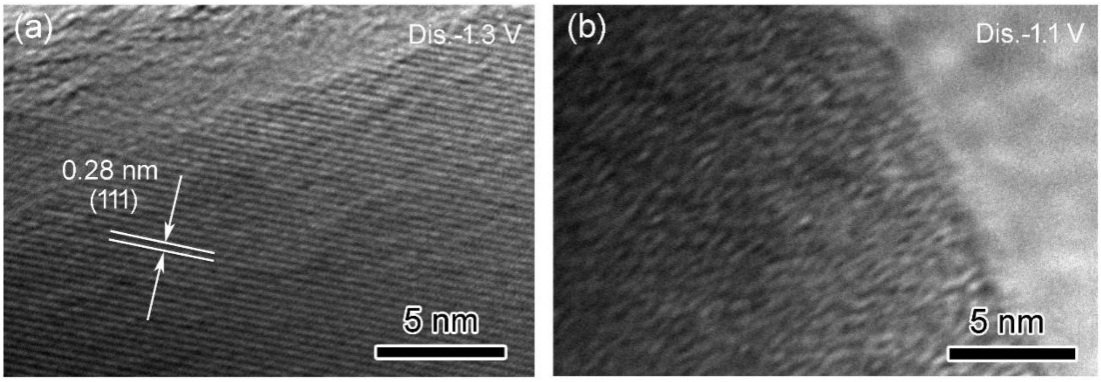

Fig. S16. HRTEM images of the PbHCF/CNTs electrode at (a) discharged to 1.3 V and (b) discharged to 1.1 V.

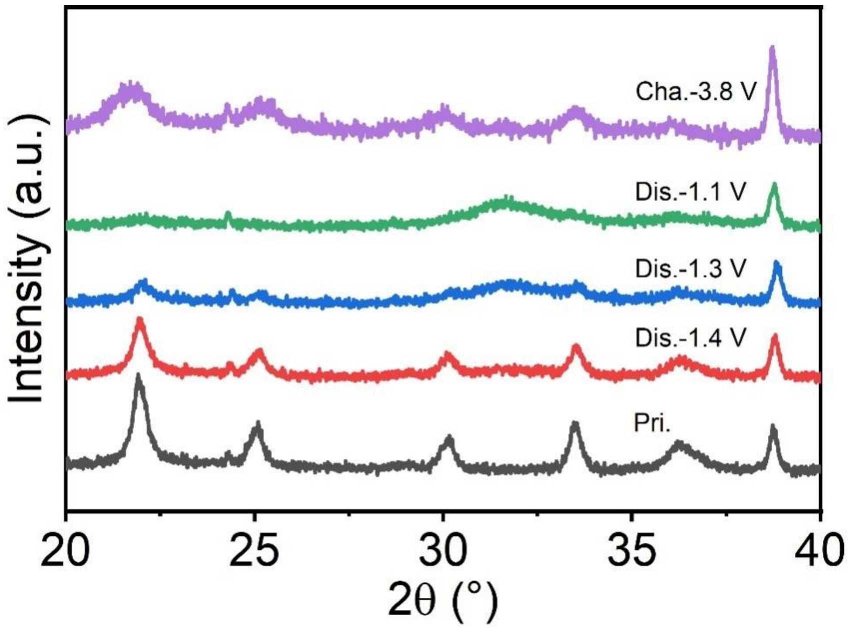

Fig. S17. Selected in situ XRD patterns of the PbHCF/CNTs cathode during the first cycle.

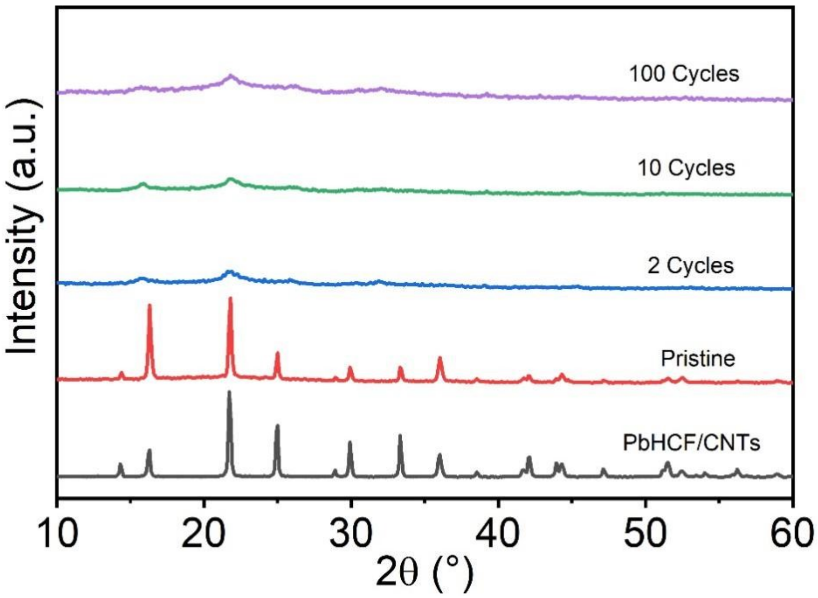

Fig. S18. XRD patterns of PbHCF/CNTs electrode at different cycles.

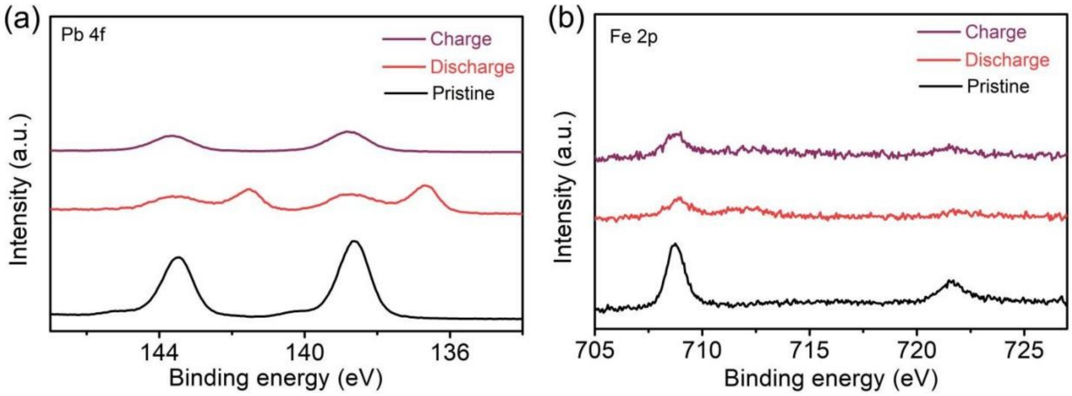

Fig. S19. XPS Pb 4f and Fe 2p spectra of PbHCF/CNTs in different charging and discharging states.

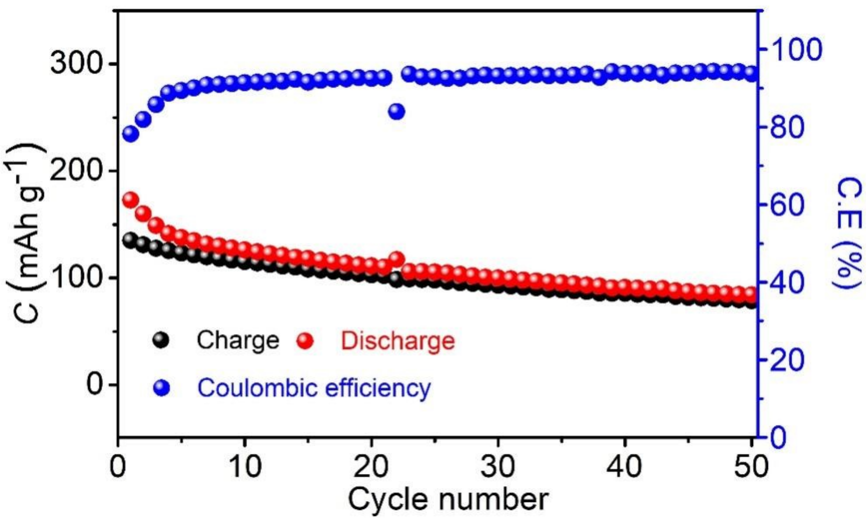

Fig. S20. Cycling performance of HC||PbHCF/CNTs full cell at 50 mA g^{-1}.

Table S1. Atomic coordinates of PbHCF.

atom	occ.	site	mult.	x	y	z
Pb	1	2d	2	0.333300	0.666700	0.600500
Fe	1	1a	1	0.000000	0.000000	0.000000
C	1	6g	6	0.065400	0.250200	0.195600
N	1	6g	6	0.301400	0.905300	0.307000

Hexagonal, a=7.163998 Å, b=7.163998 Å, c=5.431422 Å, α=γ=90°, β=120°, V=241.41 $Å^3$, (R_{wp}= 8.50%, R_p=6.68%).

Table S2 ICP-OES results of PbHCF/CNTs.

Sample	Pb(w%)	Fe(w%)	Pb/Fe
PbHCF/CNTs	69.43	9.83	1.89

Table S3 Comparison of PbHCF/CNTs sample with reported PBA-based cathodes in SIBs.

Material	Electron transferred number	Redox active site	Voltage (V vs. Na^+/Na)	Capacity ($mAh\ g^{-1}/mA\ g^{-1}$)	Ref.
PbHCF/CNTs	4	Pb^{2+}/Pb^0	1.1-3.8	161.8/20	This Work
VHCF	1	Fe^{3+}/Fe^{2+}	2.0-4.0	64/15	3
AgHCF	4	Ag^+/Ag, Fe^{3+}/Fe^{2+}	1.1-4.1	118/100	4
ZnHCF	1	Fe^{3+}/Fe^{2+}	2.0-4.2	62/8.5	5
NiHCF	1	Fe^{3+}/Fe^{2+}	2.0-4.2	80/15	6
CoNiHCF	2	Co^{3+}/Co^{2+}, Fe^{3+}/Fe^{2+}	2.0-4.2	142/30	7
FeHCF	2	Fe^{3+}/Fe^{2+}	2.0-4.35	123.41/12.2	8
BiHCF	3	Bi^{3+}/Bi^0	1.2-4.2	100.5/100	9
CuHCF	1	Fe^{3+}/Fe^{2+}	2.0-4.2	79.5/8.5	10
NiMnHCF	2	Mn^{3+}/Mn^{2+}, Fe^{3+}/Fe^{2+}	2.0-4.1	122/20	11
TiHCF	1	Fe^{3+}/Fe^{2+}	2.0-4.2	74/5	12
MnFeHCF	2	Mn^{3+}/Mn^{2+}, Fe^{3+}/Fe	2.0-4.0	164.5/10	13

References

[1] Kresse G.; Eurthmüller J. Efficiency of ab-initio total energy calculations for metals and semiconductors using a plane-wave basis set. *Comput. Mater.*, 1996, *6*, 15-50.

[2] Kresse G.; Furthmüller J. Efficient iterative schemes for ab initio total-energy calculations using a plane-wave basis set. *Phys. Rev. B*, 1996, *54*, 11169-11186.

[3] Pan Z.-T.; He Z.-H.; Hou J.-F.; Kong L.-B. Sodium vanadium hexacyanoferrate as a high-rate capability and long-life cathode material for Na-ion batteries. *J. Energy Storage*, 2022, 53, 105165.

[4] Zhao X.; Liu N.; Zheng M.; Wang X.; Xu Y.; Liu J.; Li F.; Wang L. Four-electron redox in Prussian blue analogues cathode material for high-performance sodium-ion batteries. *ACS Energy Lett.*, 2024, 9, 2748-2757.

[5] Pan Z.; Xu Y.; Li M.-P.; Kong L.-B. Sodium zinc hexacyanoferrate: A Prussian blue analog with long life. *ACS Sustainable Chem. Eng.*, 2024, 12, 13840-13847.

[6] Rehman R.; Peng J.; Yi H.; Shen Y.; Li C.; Fang C.; Li Q.; Han J. Highly crystalline nickel hexacyanoferrate as a long-life cathode material for sodium-ion batteries. *RSC Adv.*, 2020, 10, 27033-27041.

[7] Zhang J.; Wan J.; Ou M. et al. Enhanced all-climate sodium-ion batteries performance in a low-defect and Na-enriched Prussian blue analogue cathode by nickel substitution. *Energy Mater.*, 2023, 3, 300008.

[8] Kim D.; Yoo H.; Park M.-S.; Kim H. Boosting the sodium storage capability of Prussian blue nanocubes by overlaying PEDOT:PSS layer. *J. Alloys Compd.*, 2019, 791, 385-390.

[9] Wang X.; Liu N.; Zheng M.; Zhao X.; Wang L. Valence switching of bismuth in ferricyanide as cathode materials for sodium-ion batteries. *J. Power Sources*, 2025, 625, 235666.

[10] Xu Y.; Wan J.; Huang L. et al. Dual redox-active copper hexacyanoferrate nanosheets as cathode materials for advanced sodium-ion batteries. *Energy Storage Mater.*, 2020, 33, 432-441.

[11] Hu P.; Peng W.; Xiao D.; Ahuja U.; Réthoré J.; Aifantis K. Concentration-Gradient Prussian blue cathodes for Na-ion batteries. *ACS Energy Lett.*, 2020, 5, 100-108.

[12] Li M.; Mullaliu A.; Passerini S.; Giorgetti M. Titanium activation in Prussian blue based electrodes for Na-ion batteries: a synthesis and electrochemical study. *Batteries*, 2021, 7, 5-16.

[13] He S.; Zhao J.; Rong X. et al. Solvent-free mechanochemical synthesis of Na-rich Prussian white cathodes for high-performance Na-ion batteries. *Chem. Eng. J.*, 2022, 428, 131083.